ISSN 0036-0244, Russian Journal of Physical Chemistry A, 2024, Vol. 98, No. 9, pp. 2123–2134. © Pleiades Publishing, Ltd., 2024.

PHYSICAL CHEMISTRY OF NANOCLUSTERS, SUPRAMOLECULAR STRUCTURES, AND NANOMATERIALS

Study on Carbon Nanotubes of Pyrolysis Carbons P for In Situ Catalytic Formation on Expanded Graphite Surface

Y. L. Wang[a,b], W. L. Zhang[a], J. B. Tu[a,*], J. K. Huang[b], and X. F. Zeng[a,b]

[a] *College of Mining Engineering, College of Materials Science and Engineering, Hebei Provincial Key Laboratory of Inorganic Nonmetallic Materials, North China University of Science and Technology, Tangshan, 063210 China*

[b] *Tangshan Guoliang Special Refractory Limited Company, Postdoctoral Workstation, Tangshan, 063021 China*

** e-mail: tujunbo@126.com*

Received September 22, 2023; revised April 7, 2024; accepted April 9, 2024

Abstract—$Fe(NO_3)_3$, $Co(NO_3)_2$, and $Ni(NO_3)_2$ catalysts were used to form carbon nanotubes in situ from expanded graphite by changing the type, concentration and carbonization temperature of the catalysts. The microstructure, modified expanded graphite functional group and oxidation temperature of the formed carbon nanotubes were detected and analyzed. The effects of catalyst concentration and type, the ratio of carbon source Carbons P to expanded graphite and heat treatment temperature on the in-situ catalytic formation of carbon nanotubes by expanded graphite were studied and characterized by X-ray diffraction (XRD), X-ray photoelectron spectrometer (XPS), Raman spectrometer (Raman), scanning electron microscope (SEM), and thermogravimetric analysis-differential scanning calorimetry (TG-DSC) in this paper. The formation mechanism and influence rule of different experimental conditions on carbon nanotubes are studied.

Keywords: expanded graphite, carbon nanotubes, in situ doping, catalytic formation

DOI: 10.1134/S0036024424701255

INTRODUCTION

Expanded graphite (EG) is a new functional carbon material. Not only EG has natural graphite's excellent properties, but also it has another own unique characteristics. As early as the early 1860s, Brodie discovered EG, but its application did not begin at once. Later, some persons researched and developed EG and got some breakthroughs [1–5].

Due to its high expansion rate, high conductivity, good adsorption properties, strong heat transfer and heat insulation ability, expanded graphite has been widely used in sealing, conductive composite material additives, water environment remediation and air pollution treatment, flame retardant and energy storage materials [6–9].

At high temperature, the volume of EG can be increased to 150 to 300 times, so the structure becomes porous and loose. Because the surface area is increased, the surface energy is improved. The adsorption property of the EG is enhanced, and the graphite can be self-embedded, increasing its resilience, softness and plasticity [10–12].

CNTS are popular one-dimensional materials, which have a special structure. CNTS's two ends are sealed, and its axial size is microns and radial size goes as far as nanometers. According to different orientations along the axis, carbon hexagons can be divided into three kinds forms which are zigzag, armchair, and spiral chiral [13–15]. CNTS have many unique mechanical, electrical and chemical properties, such as light in weight, perfectly because of its hexagonal structure. In recent years, people pay more and more attention to CNTS and nanomaterials. CNTS are being used more and more widely [16–19].

Recently, CNTs@EG composite materials were prepared and studied. When heated in furnace, CNTs were grown on the EG surface. As catalysts, $Fe(NO_3)_3$, $Co(NO_3)_2$, and $Ni(NO_3)_2$ were used to detect and analyze the microstructure, functional groups and oxidation temperature of modified expanded graphite, and to study the formation mechanism and influence rule of different experimental conditions such as catalyst type, concentration and carbonization temperature on the in-situ catalytic formation of carbon nanotubes on the surface of expanded graphite.

2. EXPERIMENTAL

2.1. Synthesis

Through adjusting sintering temperature, catalyst types, as well as composite ratio and concentration of Carbons P in EG, a series of CNTs@EG composite samples were synthesized by high temperature reaction method.

The analytical grade raw materials of $Co(NO_3)_2{\cdot}6H_2O$ (Tianjin Yongda Chemical Reagent Co., Ltd., Tianjin, China), $Fe(NO_3)_3{\cdot}6H_2O$ (Tianjin Yongda Chemical Reagent Co., Ltd., Tianjin, China), $Ni(NO_3)_2{\cdot}6H_2O$ (Tianjin Yongda Chemical Reagent Co., Ltd., Tianjin, China), and expanded graphite (Jixi Dingyuan graphite Co., Ltd., Jixi, China) were homogeneous mixed and put into crucibles, which were heated to different sintering temperatures in a furnace.Then the mixtures were kept at the sintering temperature for some time. Finally, the resulting samples were naturally cooled to room temperature.

During the above experiment, four influencing factors, such as, catalyst types, catalyst concentration, proportioning ratio of Carbons P in EG, and carbonization temperature, were investigated for their effects on the formation of carbon nanotubes.

According to the relevant research references and the 2017 Hebei Natural Science Foundation project we completed above, the catalyst concentration and the ratios of Carbons P and EG were determined. The first is to estimate the specific surface area of EG and the amount of hydrocarbon gas released during carbonization of Carbons P. It is expected that carbon nanotubes can grow at the active sites of adsorbed catalysts on the surface of EG. Second, on the basis of this design, the pre-experiment is carried out, and the Carbons P and EG ratio is finally selected. According to the relevant research references and the 2017 Hebei Natural Science Foundation project we completed above, the catalyst concentration and the ratios of Carbons P and EG were determined. The first is to estimate the specific surface area of EG and the amount of hydrocarbon gas released during carbonization of Carbons P. It is expected that carbon nanotubes can grow at the active sites of adsorbed catalysts on the surface of EG. Second, on the basis of this design, the pre-experiment is carried out, and the Carbons P and EG ratio is finally selected according to the test results [20, 21].

Three kinds of catalyst were adopted in this experiment, which are $Fe(NO_3)_3{\cdot}6H_2O$, $Co(NO_3)_2{\cdot}6H_2O$, and $Ni(NO_3)_2{\cdot}6H_2O$, respectively. The concentrations of catalyst were set to 0, 0.5, 1.0, and 1.5%, respectively. The composite ratios of Carbons P and EG were set to 333 : 1, 500 : 1, and 666 : 1, respectively. Three kinds of carbonization temperatures were set to 1000, 1100, and 1200°C, respectively. There are four kinds of experimental designs in this experiment. First, the catalyst concentration 1.0 wt %, proportioning ratio of Carbons P and Expanded graphite 666 : 1 and carbonization temperature 1100°C remain unchanged, and types of catalyst change. Second, the type of catalyst $Co(NO_3)_2{\cdot}6H_2O$, the catalyst concentration 1.0 wt %, and carbonization temperature 1100°C remain unchanged, and the proportioning ratios of Carbons P to EG change. Third, the type of catalyst $Co(NO_3)_2{\cdot}6H_2O$, proportioning ratio of Carbons P to EG 666 : 1 and carbonization temperature 1100°C remain unchanged, the catalyst concentrations change. At last, the type of catalyst $Co(NO_3)_2{\cdot}6H_2O$, the catalyst concentration 1.0 wt %, the proportioning ratios of Carbons P to EG 666 : 1 remain unchanged, and carbonization temperature change [22–26].

2.2. Characterization

The XRD patterns of the samples were operated using a Bruker D8 Advance with CuK_α radiation (λ = 1.5418 Å) at scan rate of 0.5 min^{-1} in 2θ range from 10° to 90°. The structure of the crystal was drawn by the Diamond software. The morphology and the element distribution was studied by the scanning electron microscopy (SEM, S-4800, Japan) with an energy disperse spectroscopy probe. Raman spectra were recorded using LabRam HR 800 Raman spectrometer. Approximately, 10 mg of each sample was excited using an Ar laser operating at 532 nm and a power of 2 mW.

The elements and valence states on the surface of the sample were analyzed by X-ray photoelectron spectroscopy (XPS, PHI-5300, USA) and the valence band positions were determined by the valence band spectrum. XPS peak 4.1 software was used for subpeak fitting, and binding energy correction was carried out based on C 1*s* = 284.6 eV.

3. RESULTS AND DISCUSSIONS

3.1. Effect of Catalyst Type on In Situ Formation of Carbon Nanotubes on Expanded Graphite Surface

The first experimental design is used to study the effect of catalyst types on the in-situ catalytic formation of carbon nanotubes by cracking Carbons P on the EG surface. The XRD pattern of samples prepared with $Fe(NO_3)_3{\cdot}6H_2O$, $Co(NO_3)_2{\cdot}6H_2O$, and $Ni(NO_3)_2{\cdot}6H_2O$ as catalysts is showed in Fig. 1.

The EG in the sample is composed of graphite phase, in which the graphite diffraction peak in the sample is the strongest when $Co(NO_3)_2{\cdot}6H_2O$ is used as catalyst, which may be related to the formation of more carbon nanotubes in the sample when the catalyst is used. In addition, diffraction peaks of iron, cobalt and nickel were also detected, indicating that all three catalysts were involved in the catalytic cracking reaction.

In order to further explore the types of iron-cobalt-nickel bonding keys, the high-resolution XPS spectra of the three samples were characterized. For all samples, the high-resolution spectrum can be fitted to three peaks. For example, it can be fitted by two spin-orbit doublet characteristics of Co^{3+} and Co^{2+} in the XPS narrow survey of Co 2*p* [27, 28]. According to Fig. 2 the XPS spectra, the valence states of $Fe(NO_3)_3{\cdot}6H_2O$, $Co(NO_3)_2{\cdot}6H_2O$, and

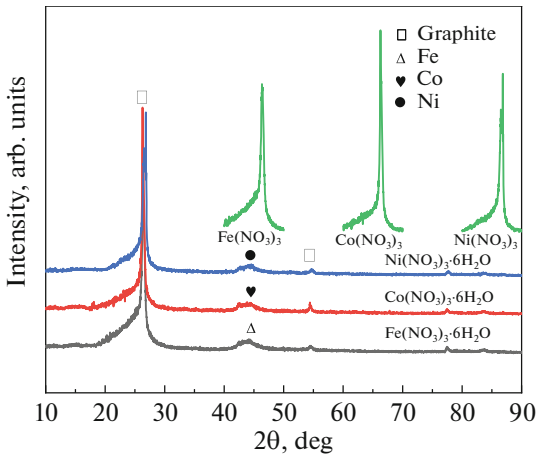

Fig. 1. The XRD patterns of the samples were prepared using $Fe(NO_3)_3{\cdot}6H_2O$, $Co(NO_3)_3{\cdot}6H_2O$, $Ni(NO_3)_2{\cdot}6H_2O$ as catalysts.

$Ni(NO_3)_2{\cdot}6H_2O$ decomposed and participated in the catalytic reaction are 0, +3, and +2. The catalyst is gradually reduced to a metal in this reaction, and it is consistent with the XRD results [29–31].

The XPS spectra of C 1*s* of metal carbides are depicted in Fig. 3. The C 1*s* spectrum is fitted to four distinct peaks, located at 280.1, 280.9, 281.3, and 287.1 eV in Fig. 3a. These peaks are respectively attributed to the C–Ni, C–Csp^2, C–Csp^3, and C–O bonds [32]. The C 1*s* spectrum is fitted to four distinct peaks at 280.6, 281.0, 282.3, and 286.2 eV, corresponding to C–Fe, C–Csp^2, C–Csp^3, and C–O, respectively [33, 34] in Fig. 3b. The C 1*s* is fitted into four distinct peaks at 279.8, 280.8, 281.3 and 282.2 eV, ascribing to C–Co, C–Csp^2, C–Csp^3, and C–O, respectively [35] in Fig. 3c. The mechanism of carbon nanotube growth in expanded graphite via catalytic pyrolysis reaction using Carbores P as carbon source have been explained in reference [36–40].

In order to evaluate the structural quality, the value of Raman D band to G band ratio was used to evaluate the structural defects in carbon. The results are shown in Fig. 4. According to the Raman spectra, when $Co(NO_3)_3{\cdot}6H_2O$, $Ni(NO_3)_3{\cdot}6H_2O$, and $Fe(NO_3)_3{\cdot}6H_2O$ were used as catalysts, ID/IG in the Raman spectra of samples were 0.409, 0.806, and 0.742, respectively. In general, the lower the Raman peak intensity ratio is, the fewer defects will occur in carbon and the higher the density of carbon structure will be. It can be seen that among the three catalysts, $Co(NO_3)_3{\cdot}6H_2O$ has the best catalytic effect.

Figures 5, 7, and 9 show the SEM images of the effects of three catalysts, $Fe(NO_3)_3{\cdot}6H_2O$, $Co(NO_3)_3{\cdot}6H_2O$, and $Ni(NO_3)_2{\cdot}6H_2O$, on the in-situ formation of carbon nanotubes on the surface of expanded graphite.

As can be seen in Figs. 5a and 5b, a certain amount of carbon nanotubes and a small amount of carbon

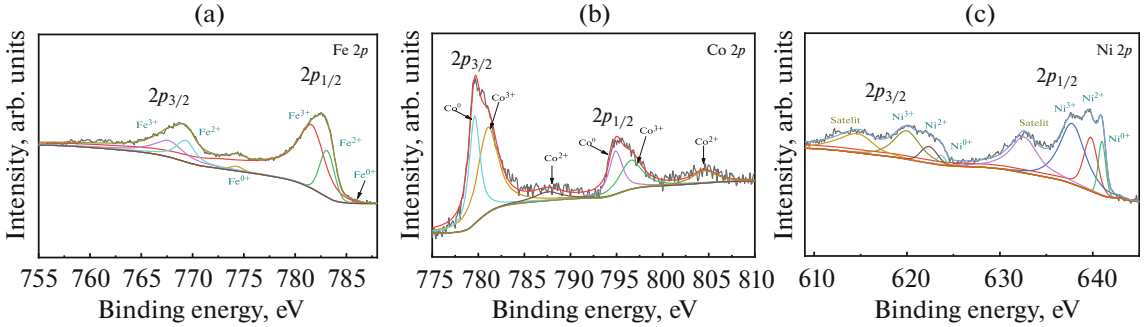

Fig. 2. XPS spectra of samples prepared with (a) $Fe(NO_3)_3{\cdot}6H_2O$, (b) $Co(NO_3)_3{\cdot}6H_2O$, and (c) $Ni(NO_3)_2{\cdot}6H_2O$ as catalysts.

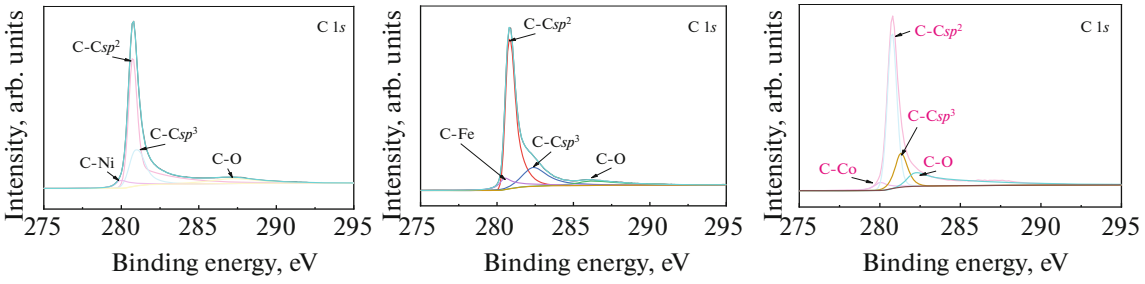

Fig. 3. XPS spectra of C 1*s* of metal carbides (a) Ni, (b) Fe, and (c) Co.

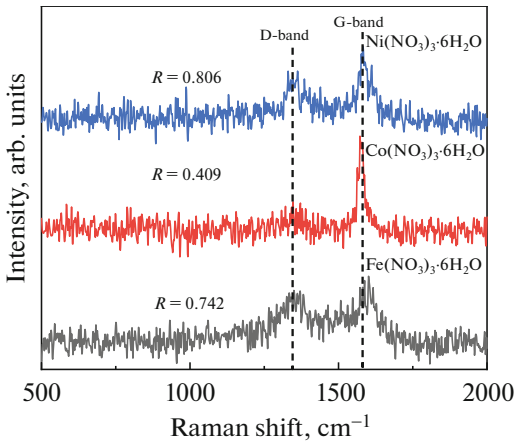

Fig. 4. The Raman spectra of the samples at different catalysts.

fiber are generated in the void of expanded graphite, with the diameter of carbon tube about 300 nm and carbon fiber about 100 nm. The carbon tube (onion carbon) in the process of development can be seen in Fig. 5c, which can be inferred to be developed from the transformation of onion carbon. The bright white substance in Figs. 5b and 5c is iron introduced by catalyst by EDS analysis. It is located at the top of the carbon tube, so it can be inferred that the growth mechanism of the carbon tube is the top growth mechanism. In addition, it can be seen from Fig. 5b that carbon tube, carbon nanotube and carbon tube prototype exist at the same time. It can be seen that carbon tube has a bamboo node structure, which is evolved from onion carbon in Fig. 5c.

In order to further observe the characteristics of the product, TEM images of the sample are shown in Fig. 6 when the catalyst is $Fe(NO_3)_3{\cdot}6H_2O$. It can be seen from Figs. 6a, 6b that the fiber structure is a multi-layer structure. According to the results of diffraction spots (Fig. 6c), the crystal structure parameters in the XRD chart of carbon nanotubes are compared, and the crystal faces (201), (200), and (102) are

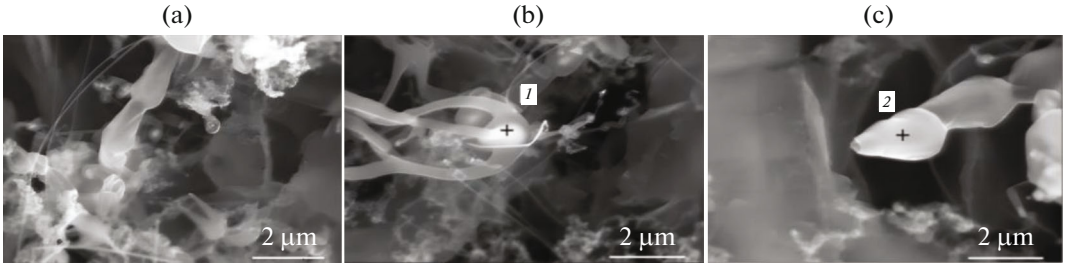

Fig. 5. SEM analysis of in-situ formation of carbon nanotubes on expanded graphite surface by catalyst $Fe(NO_3)_3{\cdot}6H_2O$.

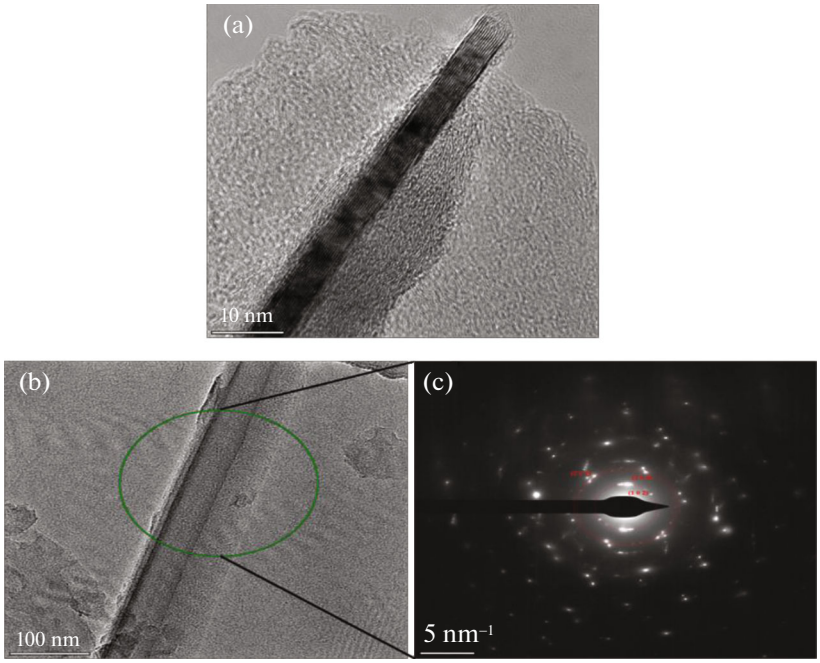

Fig. 6. TEM image of carbon nanotubes formed in situ on expanded graphite surface with $Fe(NO_3)_3{\cdot}6H_2O$ catalyst.

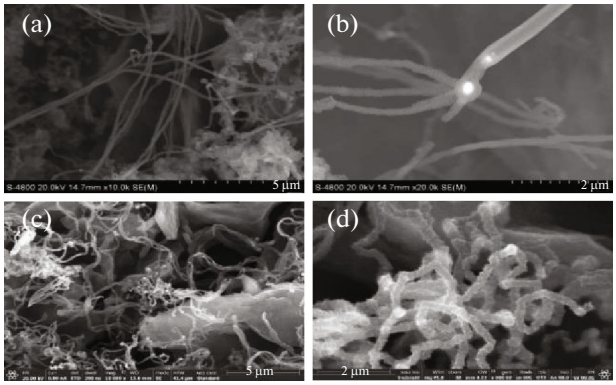

Fig. 7. SEM analysis of in-situ formation of carbon nanotubes on expanded graphite surface by catalyst $Co(NO_3)_3{\cdot}6H_2O$.

Fig. 8. TEM image of carbon nanotubes formed in situ on expanded graphite surface by $Co(NO_3)_2{\cdot}6H_2O$ catalyst.

marked, respectively, which can confirm the existence of carbon nanotubes in the experiment.

As can be seen, a large number of carbon nanotubes are generated between the spaces of the expanded graphite in Fig. 5. Carbon fibers and carbon tubes are formed in a radial manner, among which the diameter of the carbon tube is larger, about 300 nm. A large number of carbon nanotubes are formed in the expanded graphite void, which is different from using $Fe(NO_3)_3{\cdot}6H_2O$ as the catalyst. In addition, the catalyst cobalt is located on top of the carbon nanotubes and carbon fibers, as shown in Fig. 7. It can be seen that carbon nanotubes are generated from the expanded graphite surface active point in Figs. 7a, 7c, 7d, and the catalyst is on the top of the carbon nanotubes (Fig. 7b), which belong to the top growth mechanism.

In order to further observe the characteristics of carbon nanotubes, TEM images of the products in the catalyst samples containing cobalt are shown in Fig. 8. The structure of multilayer carbon nanotubes can be clearly seen in the figure. Carbon nanotubes are about 8 nm in diameter.

As exhibited in Fig. 9, when $Ni(NO_3)_2{\cdot}6H_2O$ is used as catalyst, carbon nanotubes are formed with a diameter about 230 nm in the expanded graphite void. Compared with the other two kinds catalysts, when $Ni(NO_3)_3{\cdot}6H_2O$ is used as catalyst, the diameter of carbon nanotubes generated on the expanded graphite surface is smaller. This depends on the catalyst ion diameter. The larger the catalyst ion diameter, the larger the carbon tube diameter and carbon fiber diameter. The ionic radii of Fe^{3+}, Co^{2+}, and Ni^{2+} are 0.0645, 0.0745, and 0.069 nm, respectively. In addition, compared with $Co(NO_3)_3{\cdot}6H_2O$ catalyst, the number of carbon nanotubes and carbon fibers formed on the expanded graphite surface is relatively reduced when $Ni(NO_3)_2{\cdot}6H_2O$ catalyst is used. The presence of nickel in the catalyst can also be got, indicating that the carbon nanotubes are also the top growth mode.

TEM images of the sample are shown in Fig. 10. It can be seen that multilayer carbon nanotubes, and the diameter of carbon nanotubes is significantly smaller, with an average diameter of 5 nm. The diffraction speckle is not clear, which may be due to insufficient crystallinity of carbon nanotubes catalyzed by Ni-containing catalyst.

DSC-TG curves of the sample with $Fe(NO_3)_3{\cdot}6H_2O$, $Co(NO_3)_2{\cdot}6H_2O$, $Ni(NO_3)_2{\cdot}6H_2O$ are shown in Fig. 11. It can be seen from the TG curve that the weight loss of the samples is basically the same when the three catalysts are used, and the maximum weight loss occurs in the range of 700–800°C. This may be mainly due to the reduction of catalyst $Co(NO_3)_2{\cdot}6H_2O$ to elemental Co after heat treatment,

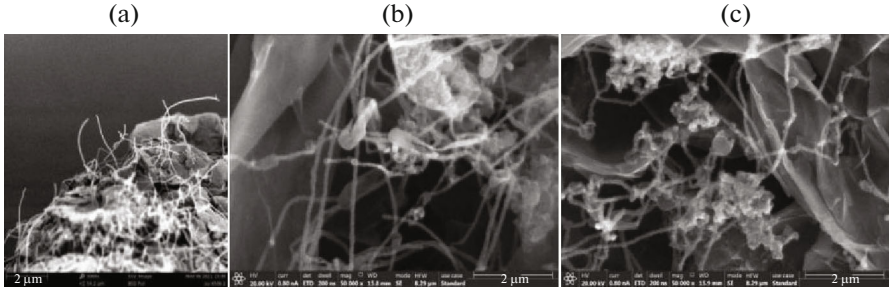

Fig. 9. SEM analysis of in-situ formation of carbon nanotubes on expanded graphite surface by catalyst $Ni(NO_3)_2{\cdot}6H_2O$ with different magnifications.

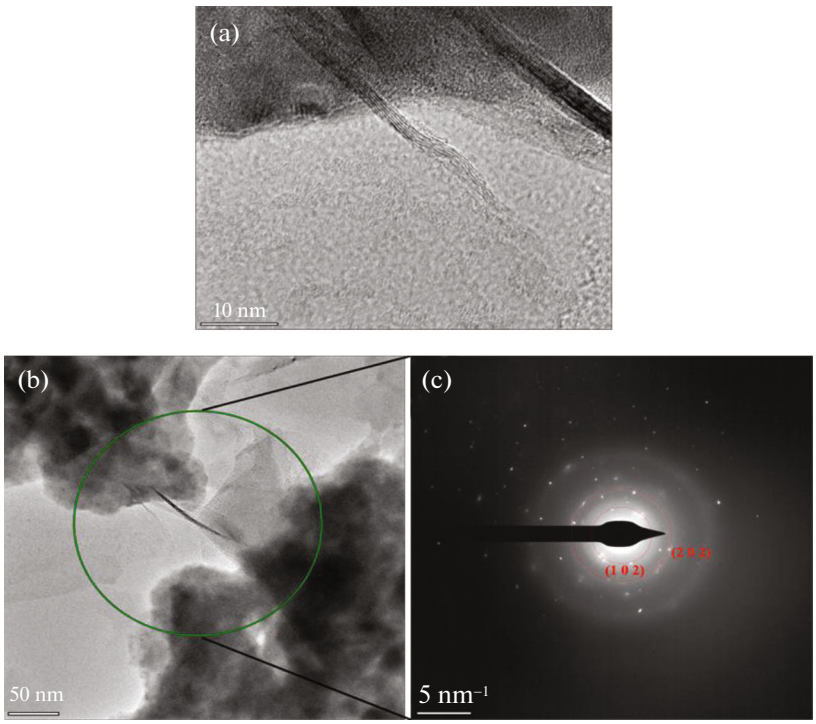

Fig. 10. TEM image of carbon nanotubes formed in situ on expanded graphite surface with $Ni(NO_3)_2{\cdot}6H_2O$ catalyst.

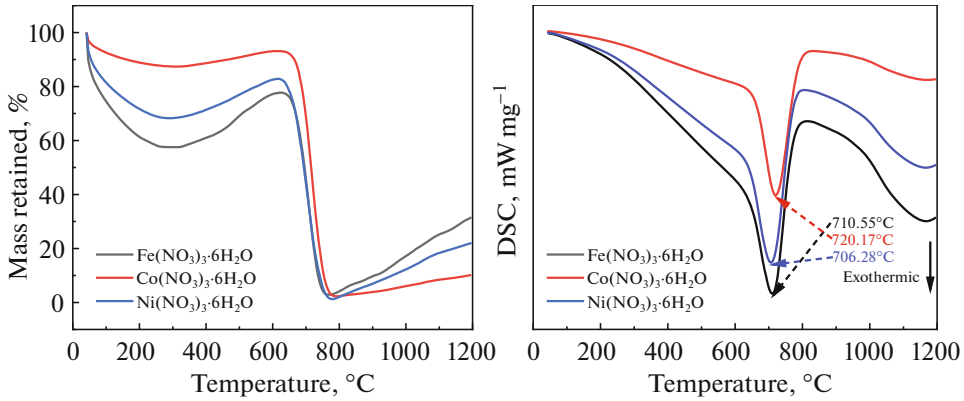

Fig. 11. DSC-TG curves of the sample with different catalysts.

and then oxidation to cobalt oxide. The reason for the weight loss of about 250°C may be that there are active points on the surface of the modified expanded graphite. During storage, hydroxyl or carboxyl groups or hydroxide plasma in the air are absorbed and heated to remove weight loss. It can be seen from the DSC curve that when $Co(NO_3)_2{\cdot}6H_2O$ is used as catalyst, the sample presents a high exothermic peak temperature, indicating that its antioxidant capacity is the best, which may be related to the more carbon nanotubes generated.

In summary, when $Co(NO_3)_2{\cdot}6H_2O$ is used as the catalyst, more carbon nanotubes are generated on the surface of expanded graphite. The higher the degree of graphitization is, the better the oxidation resistance is. In addition, when $Fe(NO_3)_2{\cdot}6H_2O$ is the catalyst, the diameter of nanotubes formed on the expanded graphite surface is larger, which may be because the larger the catalyst ion diameter, the larger the carbon tubes diameter and carbon fibers diameter.

3.2. Effect of Carbon Source and Expanded Graphite Mixture Ratio on In-Situ Formation of Carbon Nanotubes on Expanded Graphite Surface

The XRD patterns of the samples prepared by different ratios of Carbons P and expanded graphite were

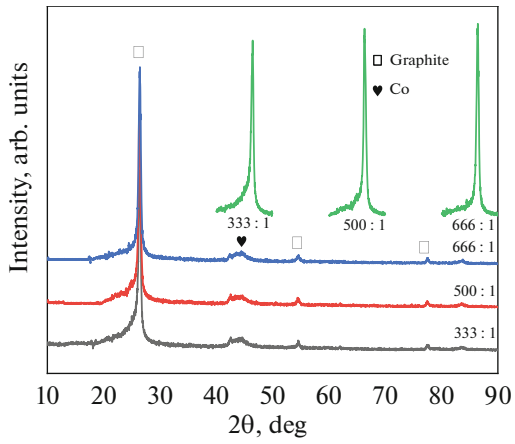

Fig. 12. The XRD patterns of the samples prepared by different ratios of Carbons P and EG.

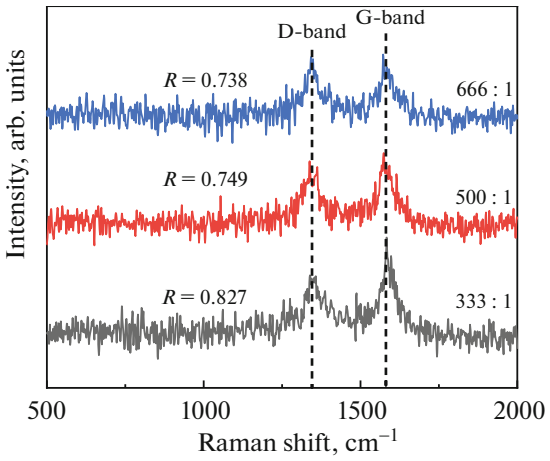

Fig. 13. The Raman spectra of the samples at different ratios of Carbons P and EG.

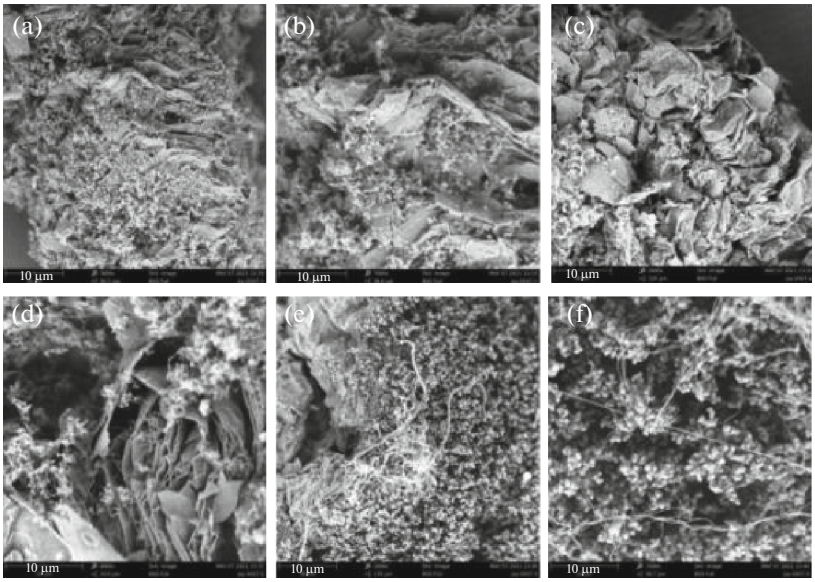

Fig. 14. SEM of the samples at different ratios of Carbons P and EG: (a, b) 333 : 1; (c, d) 500 : 1; (e, f) 666 : 1.

shown in Fig. 12. As can be seen from Fig. 12, as the ratio of carbon source carbons to expanded graphite ratio increases, the intensity of graphite characteristic diffraction peak in the sample becomes more obvious, indicating that the degree of graphitization of the sample increases. In addition, the characteristic peaks of metal Co are also enhanced, which may be related to the fact that the increase of carbon source carbons can provide more carbon sources and help catalyze the reaction.

Figure 13 shows the Raman spectra of carbons prepared by different ratio of Carbons P to expanded graphite. As the ratio of carbons increases, the R-value shows a decreasing trend. This indicates that in the case of a ratio of 666 : 1, more carbon nanotubes may be generated, thus giving the sample a higher quality carbon structure.

In order to further analyze the effect of the amount of Carbons P on the in-situ formation of carbon nanotubes on the surface of expanded graphite, the SEM images of samples prepared by different ratios of Carbons P and expanded graphite are shown in Fig. 14. From Fig. 14, as the ratio of Carbons to expanded graphite increases, the carbon microspheres formed in the expanded graphite voids gradually increase. When the ratio is 333 : 1, no carbon nanotubes or carbon fibers can be seen on the expanded graphite surface. When the ratio of ingredients is 500 : 1, the fiber material formed on the expanded graphite surface is small, and the length-diameter ratio is not large. When the ratio is 666 : 1, there are many carbon microspheres on the expanded graphite surface, and a fibrous substance with a large length-diameter ratio is formed. Since the

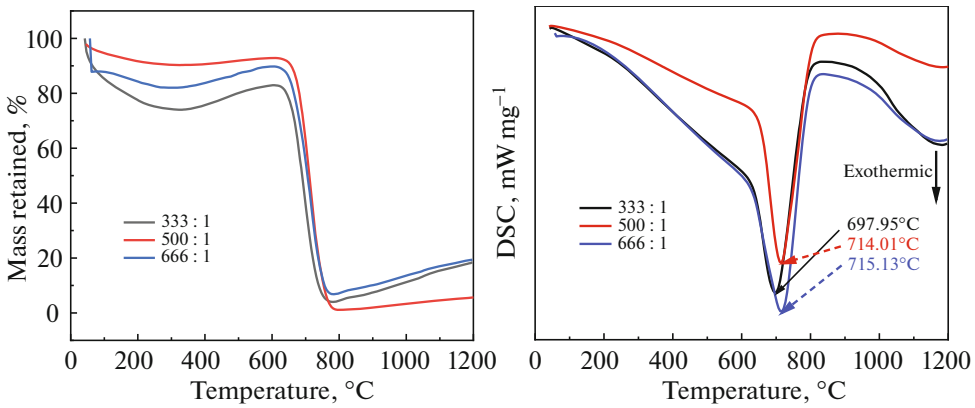

Fig. 15. TG-DSC spectra of the samples at different ratios of Carbons P and EG (a, b) 333 : 1; (c, d) 500 : 1; (e, f) 666 : 1.

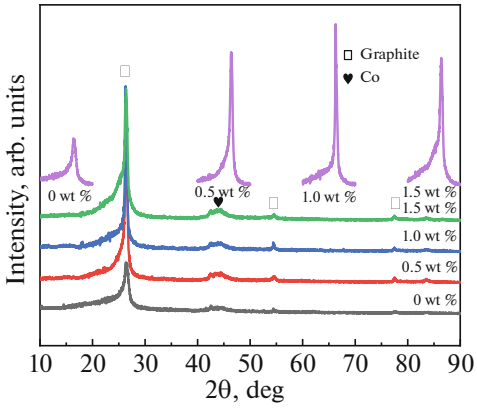

Fig. 16. The XRD pattern of samples prepared by catalyst $Co(NO_3)_2{\cdot}6H_2O$ with different concentrations.

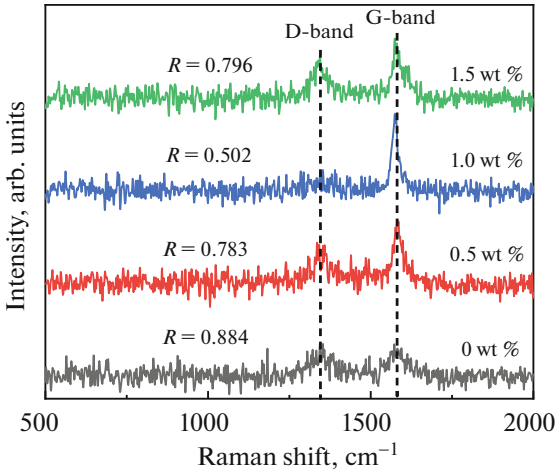

Fig. 17. The Raman spectra of samples prepared with different concentrations of catalyst $Co(NO_3)_2{\cdot}6H_2O$.

generation of carbon fiber requires enough carbon source gas, the larger the proportioning ratio, the more carbon source gas can be provided, and the easier it is to form carbon fiber like substances. Therefore, the following experiment determines that the ratio of ingredients is 666 : 1.

The TG-DSC spectra of different ratio of Carbons P to expanded graphite are shown in Fig. 15. It can be seen from the TG diagram that the weight loss of the sample is the largest when the ratio of ingredients is 500 : 1. The sample showed the least weight loss when the ratio of ingredients was 666 : 1. It can be seen from the DSC map that the temperature corresponding to the exothermic peak of the sample is the highest when the ratio is 666 : 1, which indicates that its antioxidant capacity is strong, which may be related to the number and morphology of carbon nanotubes generated in the sample.

It can be seen that the carbon nanotubes generated in the sample have the best quality when the Carbons P to expanded graphite ratio is 666 : 1. The degree of graphitization of the sample is high, showing better antioxidant capacity.

3.3. The Effect of Catalyst Concentration on the In-Situ Catalytic Formation of Carbon Nanotubes on the Surface of Expanded Graphite

The XRD pattern of samples prepared by catalyst $Co(NO_3)_2{\cdot}6H_2O$ with different concentrations are shown in Fig. 16. As can be seen from Fig. 12, with the increase of catalyst $Co(NO_3)_2{\cdot}6H_2O$ concentration, the diffraction peak of graphite phase in the sample first increased and then decreased. When the concentration of catalyst $Co(NO_3)_2{\cdot}6H_2O$ increased from 0 to 0.5 wt % to 1.0 to 1.5 wt %, the intensity of metal Co corresponding to the diffraction peak showed a trend of first increasing and then decreasing, which indicated that when the catalyst concentration was 1.0 wt %, the carbon nanotubes generated in the sample were the most.

The Raman spectra of samples prepared with different concentrations of catalyst $Co(NO_3)_2{\cdot}6H_2O$ are shown in Fig. 17. As can be seen from Fig. 17, when the catalyst concentration is 1.0 wt %, the minimum R value is 0.502, indicating that there are more carbon

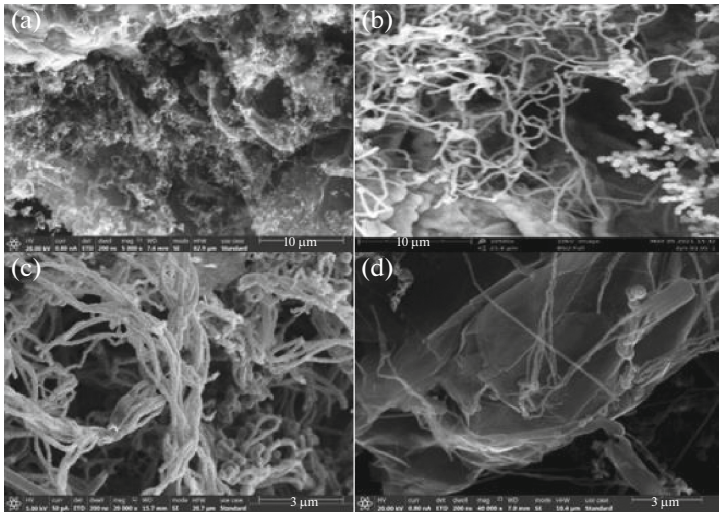

Fig. 18. The SEM of samples prepared with different concentrations of catalyst $Co(NO_3)_2{\cdot}6H_2O$ (a) 0, (b) 0.5, (c) 1.0, and (d) 1.5 wt %.

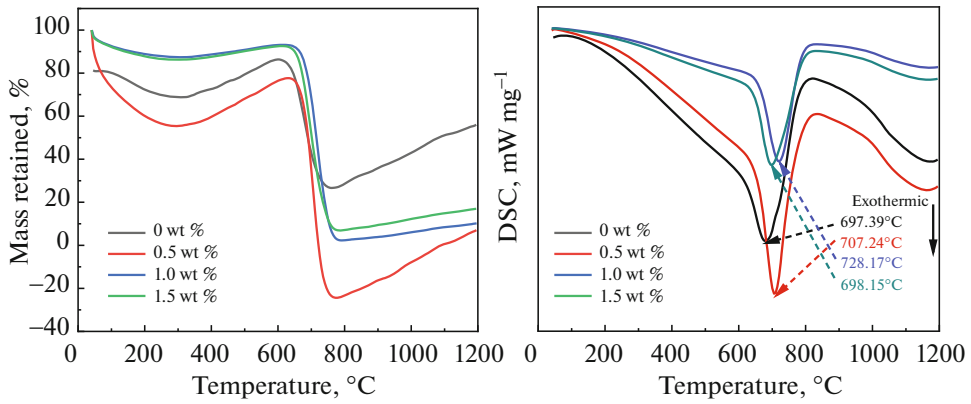

Fig. 19. TG-DSC spectra of samples prepared by catalyst $Co(NO_3)_2{\cdot}6H_2O$ at different concentrations.

nanotubes growing on the surface of expanded graphite and the least defects of expanded graphite.

The SEM of samples prepared with different concentrations of catalyst $Co(NO_3)_2{\cdot}6H_2O$ are shown in Fig. 18. As can be seen from Fig. 18, when no catalyst $Co(NO_3)_2{\cdot}6H_2O$ is added, no carbon nanotubes are found in the expanded graphite void. When the catalyst $Co(NO_3)_2{\cdot}6H_2O$ content is 0.5 wt %, carbon microspheres and nanofibers are formed between the expanded graphite, and they are connected with each other. When the catalyst $Co(NO_3)_2{\cdot}6H_2O$ content is 1.0 wt %, a large number of carbon nanotubes are formed in the expanded graphite void, which are intertwined with each other. When the amount of catalyst is 1.5 wt %, less carbon nanotubes are formed in the expanded graphite void. This may be due to the adsorption of carbon atoms from one side of the catalyst to the other side, when the amount of catalyst is more, the diffusion path of carbon atoms becomes larger, which is not conducive to the growth of carbon nanotubes.

TG-DSC spectra of samples prepared by catalyst $Co(NO_3)_2{\cdot}6H_2O$ at different concentrations are shown in Fig. 19. According to the DSC curve, when the catalyst concentration is 1.0 wt %, the exothermic peak temperature on the DSC curve reaches 720.17°C. The results show that the carbon nanotubes can improve the oxidation resistance of the expanded graphite. According to the TG diagram, when the catalyst concentration is 0.5 wt %, the weight loss reaches 85%. At the catalyst concentration of 1 wt %, the weight loss reached 84%.

In summary, when no catalyst $Co(NO_3)_2{\cdot}6H_2O$ is added, it is difficult to form carbon nanotubes on the expanded graphite surface. When the concentration of catalyst $Co(NO_3)_2{\cdot}6H_2O$ is 1.0 wt %, more carbon nanotubes grow on the surface of expanded graphite, resulting in fewer defects, high graphitization degree

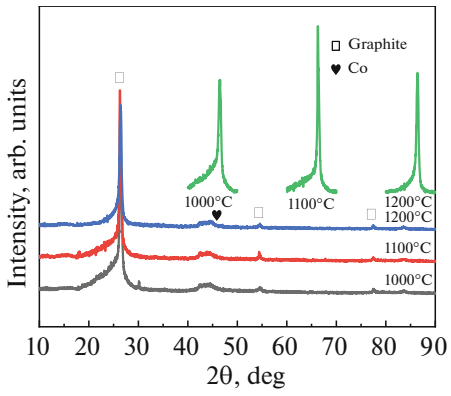

Fig. 20. The XRD pattern of the sample prepared at different heat treatment temperatures.

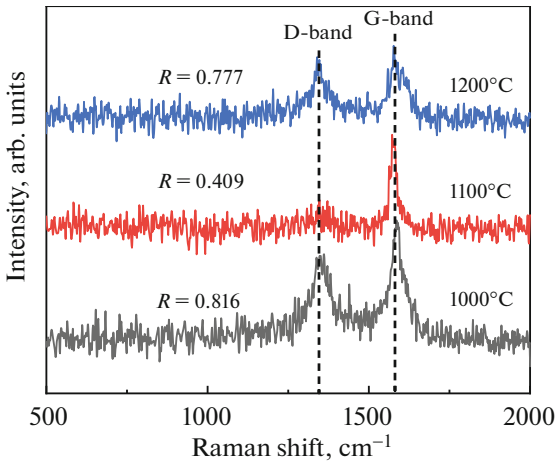

Fig. 21. The Raman spectra of carbon nanotubes samples prepared at different heat treatment temperatures.

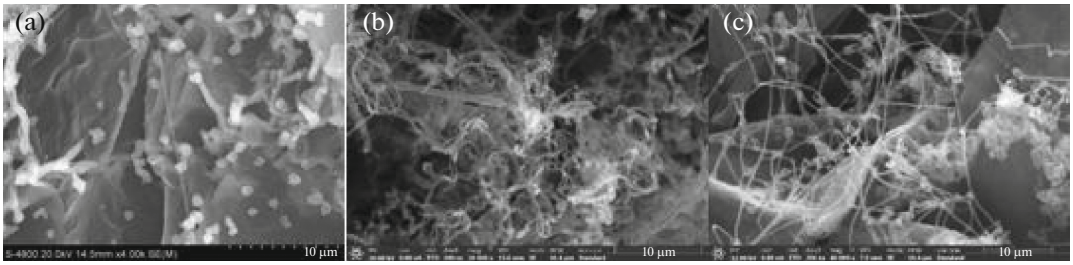

Fig. 22. SEM spectra of carbon nanotubes prepared at different heat treatment temperatures (a) 1000, (b) 1100, and (c) 1200°C.

and the best antioxidant capacity. When the catalyst concentration is 1.5 wt %, the carbon nanotubes generated on the expanded graphite surface are less, indicating that the catalyst concentration of 1.0 wt % is more appropriate.

3.4. Effect of Heat Treatment Temperature on In-Situ Formation of Carbon Nanotubes on Expanded Graphite Surface

The XRD patterns of the sample prepared at different heat treatment temperatures are shown in Fig. 20. It can be seen that the XRD pattern of the sample increases as the heat treatment temperature increases from 1000 to 1100°C, indicating that more carbon nanotubes may be generated at this time, which promotes the graphitization of the sample. When the heat treatment temperature continued to rise to 1200°C, the degree of graphitization in the sample decreased.

Figure 21 shows the Raman spectra of Carbon nanotubes samples prepared at different heat treatment temperatures. As can be seen from Fig. 21, the minimum R-value is 0.409 at 1100°C. It shows that at 1100°C, more carbon nanotubes are generated, so that the expanded graphite has the least defects and the highest quality.

SEM spectra of carbon nanotubes prepared at 1000, 1100, and 1200°C are shown in Fig. 22. As can be seen from Fig. 22, when the heat treatment temperature is 1000°C, a large number of carbon microspheres and a small number of carbon tubes are formed in the void and surface of expanded graphite. This may be because the heat treatment temperature is not high, the catalyst activity is low, and then affect the nucleation and growth of carbon nanotubes. Carbon atoms are mostly deposited on the catalyst surface to form carbon spheres. When the heat treatment temperature is 1100°C, a large number of carbon nanotubes are formed on the expanded graphite surface. This is because the catalyst activity is high at this temperature, the carbon atoms in the catalyst particles are easy to reach saturation, and the rate of carbon atom adsorption and the rate of carbon atom precipitation can be in a state of equilibrium, so that the carbon nanotubes are easy to nucleate and grow. When the heat treatment temperature is 1200°C, the carbon atoms generated by the pyrolysis of carbons will be deposited on the surface of the expanded graphite in the form of activated carbon, which will wrap the catalyst and make it inactive, so that it is difficult to generate carbon nanotubes, resulting in a decrease in carbon nanotube generation.

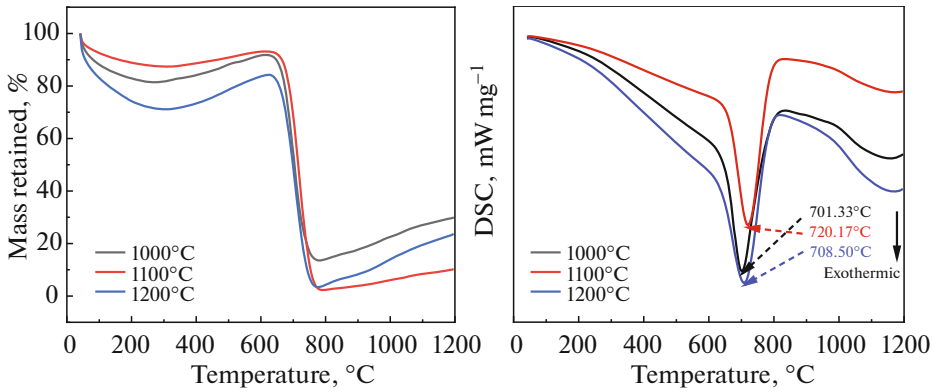

Fig. 23. The TG-DSC spectra of the samples prepared at different carbonization temperatures.

The TG-DSC spectra of the samples prepared at different carbonization temperatures are shown in Fig. 23. According to the TG curve, when the heat treatment temperature is 1100°C, the weight loss reaches 85 wt %. In the DSC curve, the sample with heat treatment temperature of 1100°C has the highest exothermic peak temperature, reaching 720.17°C, and the integral area of exothermic peak is the smallest. The results indicate that the expanded graphite has better oxidation resistance due to the formation of a large number of carbon nanotubes after heat treatment at 1100°C.

It can be seen that compared with 1000 and 1200°C, the heat treatment temperature of 1100°C is conducive to the formation of carbon nanotubes on the surface of expanded graphite, thus improving the antioxidant capacity of the sample.

CONCLUSIONS

In this experiment, the expanded graphite catalyzed in situ to form carbon nanotubes was prepared by vacuum impregnation of the expanded graphite with catalyst solution combined with chemical vapor deposition. The effects of catalyst type, Carbores P ratio of carbon source to expanded graphite, catalyst concentration, heat treatment temperature and other factors on the in-situ formation of carbon nanotubes on the surface of expanded graphite were studied. The mechanism of forming carbon nanotubes on the expanded graphite surface was discussed. It can be learned from the experiment that the best catalyst is cobalt nitrate, and the catalytic ability is better when the catalyst concentration is 1.0 wt %. Carbons: the optimal ratio of expanded graphite is 666 : 1, at which point the carbon nanotubes grown will be of the best quality; under the experimental conditions, the most suitable temperature for the in-situ catalytic formation of carbon nanotubes on the surface of expanded graphite is 1100°C.

AUTHOR CONTRIBUTION

All author contributed equally to the paper.

FUNDING

This work was financially supported by the Natural Science Foundation of Hebei Province of China (grant nos. E2017209164 and E2023209035) and Tangshan New High Temperature Materials Innovation Consortium Capacity Enhancement Project (grant no. 22150239J).

CONFLICT OF INTEREST

The authors of this work declare that they have no conflicts of interest.

REFERENCES

1. A. Celzard, J. F. Mareche, and G. Furdin, Prog. Mater. Sci. **50**, 93 (2005).
2. D. D. L. Chung, Carbon **39**, 279 (2001).
3. N. Wang, L. Li, Y. Xu, et al., Polym. Polym. Compos. **28**, 209 (2020).
4. Z. Cheng, D. J. Liao, X. Hu, et al., Polym. Degrad. Stab. **178**, 109201 (2020).
5. T. Guo, R. Zhang, X. Wang, et al., Molecules **27**, (2022).
6. J. Wei, L. Zhao, Q. Zhang, et al., Energy Build. **159**, 66 (2018).
7. J. Wei, Z. Miao, Y. Wang, et al., Energy Build. **254**, 111671 (2022).
8. Y. Huang and C. Wan, J. Adv. Ceram. **9**, 271 (2020).
9. B. Hao, Z. Tao, X. Yan, et al., Carbon **196**, 540 (2022).
10. J. Wei, Wang, X. Li, et al., Int. J. Energy Res. **44**, 6885 (2020).
11. B. Xing, J. Zhao, Y. Ren, et al., Inorg. Chem. Commun. **137**, 109185 (2022).
12. Y. Su, N. Chen, H. L. Ren, et al., Carbon Lett. **33**, 1 (2023).
13. S. K. Behera and B. Mishra, Ceram. Int. **41**, 4254 (2015).

14. Q. Wang, Y. Li, S. Sang, et al., J. Alloys Compd. **645**, 388 (2015).
15. L. X. Li, Z. W. Song, X. K. Shi, et al., Adv. Mater. Res. **777**, 43 (2013).
16. M. Luo, Y. Li, S. Jin, et al., Mater. Sci. Eng. A **548**, 134 (2012).
17. S. Saconsint, N. Saetang, A. Srifa, et al., Sci. Rep. **12** (2022).
18. Y. A. Ince, M. Tanoglu, S. Yilmaz, et al., Turk. J. Chem. **44**, 1002 (2020).
19. J. Zuo, W. Yao, and K. Wu, Fulleren. Nanotub. Carbon Nanostruct. **23**, 383 (2015).
20. B. J. Tang, Master's Thesis (North China Univ. Sci. Technol., Tangshan, 2019).
21. J. Y. Li, Master's Thesis (North China Univ. Sci. Technol., Tangshan, 2018).
22. Z. Pápa, E. Kecsenovity, D. Fejes, et al., Appl. Surf. Sci. **885**, 428 (2018).
23. S. Darban, M. G. Kakroudi, M. B. Vandchali, et al., Ceram. Int. **13**, 46 (2020).
24. W. Guo and S. L. An, Bull. Chin. Ceram. Soc. **5**, 26 (2007).
25. H. Wang, Y. W. Li, S. B. Sang, et al., Bull. Chin. Ceram. Soc. **33** (2014).
26. Z. Y. Wang, J. C. Wei, X. Y. Zheng, et al., Refract. Mater. **2**, 55 (2021).
27. H. Yang, M. Zhu, X. Guo, et al., ACS Omega **4**, 22325 (2019).
28. H. Gao, Y. Liu, Y. Ma, et al., Ionics **27**, 2561 (2021).
29. Q. Wang, Y. Li, N. Liao, et al., Ceram. Int. **43**, 16710 (2017).
30. Q. Wang, Y. Li, S. Jin, et al., Mater. Sci. Eng. A **709**, 160 (2018).
31. S. Mahato and S. K. Behera, Ceram. Int. **42**, 7611 (2016).
32. R. F. André, L. Meyniel, et al., Catal. Sci. Technol. **12** (2022). https://doi.org/10.1039/d2cy00894g
33. A. I. Alharthi, T. F. Qahtan, M. N. Shaddad, et al., Nano Mater. (Basel) **13**, 2461 (2023). https://doi.org/10.3390/nano13172461
34. N. A. Zubir, C. Yacou, J. Motuzas, X. Zhang, et al., Sci. Rep. **4594**, 4 (2014). https://doi.org/10.1038/srep04594
35. Q. Guo, J. Mao, S. Li, et al., Nano Mater. (Basel) **12**, 3388 (2022). https://doi.org/10.3390/nano12193388
36. Y. L. Wang, W. L. Zhang, Y. J. Chen, et al., Front Chem. **1** (2023). https://www.frontiersin.org/articles/10.3389/fchem.2023.1260099/full
37. Y. S. Nechaev, E. A. Denisov, A. O. Cheretaeva, et al., J. Carbon Res. **8** (2), 23 (2022).
38. M. M. Ardestani, S. Mahpishanian, B. F. Rad, et al., Korean J. Chem. Eng. **39**, 1496 (2022).
39. M. R. Gomes, T. Leber, T. Tillmann, et al., J. Eur. Ceram. Soc. **44**, 1307 (2024).
40. A. Kumar, K. Sharma, and A. R. Dixit, Carbon Lett. **31**, 149 (2021).